Applied Radiation and Isotopes 129 (2017) 28–34

Contents lists available at ScienceDirect

Applied Radiation and Isotopes

journal homepage: www.elsevier.com/locate/apradiso

Energy distribution of the neutron flux measurements at the Chilean Reactor RECH-1 using multi-foil neutron activation and the Expectation Maximization unfolding algorithm

F. Molina[a,*], P. Aguilera[b,a], J. Romero-Barrientos[c,a], H.F. Arellano[c], J. Agramunt[d], J. Medel[a], J.R. Morales[b], M. Zambra[a,e]

[a] Comisión Chilena de Energía Nuclear, Nueva Bilbao 12501, Las Condes, Santiago, Chile
[b] Facultad de Ciencias, Departamento de Física, Universidad de Chile, Las Palmeras 3425, Ñuñoa, Santiago, Chile
[c] Departamento de Física-FCFM, Universidad de Chile, Av. Blanco Encalada 2008, Santiago, Chile
[d] Instituto de Física Corpuscular (IFIC), CSIC-Univ. Valencia, Apdo. 22085, E-46071 Valencia, Spain
[e] Universidad Diego Portales, Manuel Rodríguez Sur 415, Santiago, Chile

HIGHLIGHTS

- Neutron Flux of the RECH-1 Chilean Reactor was experimentally obtained.
- Self-shielding factor per each neutron energy group was obtained using MCNP.
- Results were compared using three neutron cross section data bases.
- Two unfolding algorithms were compared: EM and GRAVEL.
- Extending the use of EM Bayes' algorithm to reactor neutron flux distributions.

ARTICLE INFO

MSC:
00–01
99-00

Keywords:
Neutron activation
Expectation maximization
Experimental reactor neutron flux distribution

ABSTRACT

We present a methodology to obtain the energy distribution of the neutron flux of an experimental nuclear reactor, using multi-foil activation measurements and the Expectation Maximization unfolding algorithm, which is presented as an alternative to well known unfolding methods such as GRAVEL. Self-shielding flux corrections for energy bin groups were obtained using MCNP6 Monte Carlo simulations. We have made studies at the at the Dry Tube of RECH-1 obtaining fluxes of $1.5(4) \times 10^{13}\ \mathrm{cm}^{-2}\,\mathrm{s}^{-1}$ for the thermal neutron energy region, $1.9(5) \times 10^{12}\ \mathrm{cm}^{-2}\,\mathrm{s}^{-1}$ for the epithermal neutron energy region, and $4.3(11) \times 10^{11}\ \mathrm{cm}^{-2}\,\mathrm{s}^{-1}$ for the fast neutron energy region.

1. Introduction

One of the most important parameters in an experimental nuclear reactor is the energy distribution of the neutron flux at the position where neutron activation experiments are carried out. Direct flux measurements are very challenging by various reasons such as the broad neutron energy range in a reactor (from 5×10^{-5} eV up to 2×10^{7} eV), neutron inelastic cross sections resonances, difficulties to place neutron detector near the reactor core, among many others.

There is not a unique approach to obtain the neutron flux energy distribution in a nuclear reactor. Indeed, several methods have been developed during the years originating mainly from the neutron activation analysis (NAA) community, such as the k_0 method, the Bonner's spheres and the multi-foil neutron activation method.

The k_0 method provides a reliable tool to obtain element concentration present in an unknown sample. It can also be used to obtain the thermal and epithermal neutron fluxes assuming that the epithemal reactor neutron flux is a fraction of the thermal flux, neglecting the fast neutron flux (Simonits, 1975). The Bonner's Spheres method requires neutron detectors such as the ^{3}He proportional counter detectors and a set of different size neutron moderator materials (polyethylene, for instance) to be sensitive to different neutron energy ranges. This method is used to measure standard neutron sources, ambient neutrons and low counting rate neutron fluxes. Nevertheless, sizes and weights of the moderator-detector set make them unsuitable for measurements near the reactor core.

* Corresponding author.
E-mail address: Francisco.Molina@cchen.cl (F. Molina).

http://dx.doi.org/10.1016/j.apradiso.2017.08.001
Received 14 June 2017; Received in revised form 25 July 2017; Accepted 2 August 2017
Available online 04 August 2017
0969-8043/

The multi-foil method is an excellent tool to obtain the neutron flux. A sample of high purity is immersed in a neutron field. After irradiation, the activity of the radioactive nuclei is measured by means of high resolution gamma spectroscopy, to obtain the saturation activity A^{∞}. This quantity can be obtained from the convolution of the reaction cross section $\sigma(E)$ with the neutron flux $\phi(E)$.

$$A^{\infty} = \int_0^{\infty} \sigma(E)\phi(E)\, dE. \tag{1}$$

To unfold $\phi(E)$ from Eq. (1) the inverse problem must be solved. It is convenient to write Eq. (1) in its discrete form as

$$A_i^{\infty} = \sum_{j=1}^{n} \sigma_{ij}\phi_j, \tag{2}$$

where the energy space is divided in n regions or groups. Here A_i^{∞} corresponds to the saturation activity measurement for the reaction i and its respective cross section matrix elements σ_{ij}.

Various techniques are available to solve the inverse problem by means of unfolding algorithms. The most used one for reactor neutron flux distributions is the Least Square with non linear model (Bitelli, 2009; Iqbal, 2009) which is included in different codes such as SAND-II (McElroy,), SANDBP (Zsolnay and Szondi,) and GRAVEL (Matzke,). Other methods are Linear regularization, Maximum Entropy and Maximum Likelihood estimation (Cvachovec and Cvachovec,).

In this work the application of Maximum Likelihood estimation using the iterative algorithm Expectation Maximization (EM) is applied to obtain, for the first time, neutron reactor flux energy distributions using neutron activation measurements. This algorithm has been successfully applied in beta decay experiments using total absorption spectroscopy (TAS) techniques, finding decay feeding probabilities (Tain and Cano-Ott, 2007), and recently to obtain the neutron background flux at the Canfranc Underground Laboratory (LSC) using ^{3}He proportional counter detectors embedded in individual polyethylene blocks of different sizes (Jordan, 2013).

Iterative Bayes' unfolding algorithms, such as the EM method, does not require a previous knowledge of the initial distribution. As a matter of fact, it is possible to start the iteration process using an uniform distribution according to Ref. D'Agostini (1995). This statement will also be tested in our work Fig. 1.

2. Multi foil neutron activation measurements

Activation measurements were carried out in the RECH-1 Dry Tube irradiation position, which facility is commonly used for neutron activation analysis at short irradiations. To access this activation position samples were positioned inside a Teflon basket container.

Nine samples of different metallic foil materials were prepared to be irradiated at the Dry Tube position at RECH-1 (see Table 1). Each sample was carefully cleaned using isopropyl alcohol and acetone.

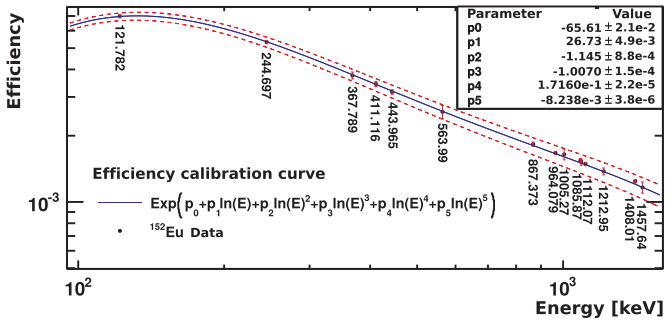

Fig. 1. Gamma efficiency curve of the HPGe detector using an ^{152}Eu source. In blue is the fitted curve from Ref. Hu (1998). Red curves represent the uncertainty given by the fitted parameters. (For interpretation of the references to color in this figure legend, the reader is referred to the web version of this article).

Table 1
Foil materials used for neutron activation at RECH-1. The purity value is given by the manufacturer. Thickness and mass of the sample were measured using an Erichsen Layer Check and a Belltronic Digital Balance model ESJ-200-4. The diameter of the samples corresponds to a standard puncher hole in accordance with ISO 838.

Sample material	Purity %	Thick. μm	Diam. mm	Mass mg	Act. time	Waiting time	Meas. time
Ti	99.99	105 (1)	3.0 (3)	4.3 (1)	10 m	5 m	5 h
V	99.8	132 (1)	6.0 (5)	21.1 (1)	10 m	43 m	38 m
Mn	98.7	60 (2)	6.0 (5)	14.1 (1)	10 m	24.6 h	47.7 h
Co	99.99	50 (5%)	6.0 (5)	12.6 (1)	10 m	42 m	100 m
Cu	99.9	142 (2)	6.0 (5)	23.4 (1)	10 m	26 m	11.7 h
Ag	99.95	144 (1)	3.0 (3)	11.7 (1)	3 m	15 m	4 h
Pd	99.9	75 (1)	3.0 (3)	5.9 (1)	10 m	27 m	2.5 d
In	99.99	118 (2)	3.0 (3)	26.6 (1)	3 m	7.2 h	2.3 h
Cd	99.9	252 (2)	6.0 (5)	60.6 (1)	9 m	65 m	104 m

Samples were exposed to a neutron flux during a time t_a. Immediately after each irradiation the sample was stored in a Lead Cell at the top of RECH-1 pool. After waiting for the decay of the activity in order to be safely transported, the irradiated sample was taken to the gamma spectrometry laboratory.

A HPGe detector (Canberra model GC2520) with a digital signal analyzer LYNX DSA Canberra, using the acquisition software GENIE 2000, was used to measure the activity of the nuclei after the neutron activation. The detector was inside a Canberra lead cylinder with cooper interior shielding. Each activated sample was positioned at 10 cm distance from the detector surface using a set of acrylic disks. In this work the acquisition was setup in Pulse Height Analysis (PHA + option in GENIE 2000) leaving the loss-free counting option off, which means that dead time correction factor must be included as is suggested in Ref. Roscoe and Furr (1977). The software was prepared to acquire γ-spectra at intervals ranging from 10 s to 10 min depending on the half-lives of the radioactive nuclei, in order to be able to obtain the dead time curve and dead time correction factor D for each irradiated sample. Efficiency calibration was measured up to 1.4 MeV using an ^{152}Eu source (Hu, 1998).

The atom-specific saturation activities were obtained according to the following expression

$$A_i^{\infty} = \frac{C(t_m)\lambda e^{\lambda t_w}}{N_0 \varepsilon_\gamma I_\gamma D(1 - e^{-\lambda t_m})(1 - e^{-\lambda t_a})} \tag{3}$$

where t_a, t_w and t_m are the irradiation, waiting and gamma-measurement time respectively (see Table 1). $C(t_m)$ denotes the net counts for the corresponding photo peak during the spectrometry measurement, λ is the decay constant of the radioactive nucleus, N_0 is the number of atoms of the isotope in the sample, ε_γ is the photo peak efficiency, I_γ is the fraction of decays producing the measured gamma-ray energy and D is the dead time correction factor calculated for nuclei whose half-lives are comparable with its respective measurement time (Roscoe and Furr, 1977). The atom-specific saturation activities are summarized in Table 2. The uncertainty of A^{∞} is given by the error propagation of the measured values: irradiation, waiting and measurement times, number of counts of the photo-peak, mass of the sample and gamma efficiency, and the reported uncertainties of I_γ and $T_{1/2}$.

3. The EM unfolding method

Bayes theorem allows to relate causes with effects. It states that it is possible to obtain an *a posteriori* probability $P(\phi_j|A_i^{\infty})$ given an *a priori* information or state of knowledge $P(\phi_j)$, in addition to the evidence given by an experiment A_i^{∞} (Tain and Cano-Ott, 2007; D'Agostini, 1995). This conditional probability is given by

$$P(\phi_j|A_i^{\infty}) = \frac{P(A_i^{\infty}|\phi_j)P(\phi_j)}{\sum_{j=1}^{n} P(A_i^{\infty}|\phi_j)P(\phi_j)}, \tag{4}$$

Table 2
Reactions studied by neutron activation at RECH-1. The thermal cross section σ_{th} evaluated at 0.025 eV, the half-life $T_{1/2}$ of the respective radioactive product of reaction, the energy of the most intense gamma line and the atom-specific saturation activity A^{∞} measured in this report are shown.

Reaction	σ_{th} barns	$T_{1/2}$	Energy keV	A^{∞} Bq/atom
^{50}Ti (n,γ)^{51}Ti	0.18	5.76 (1) m	320	$8.7(11) \times 10^{-13}$
^{51}V (n,γ)^{52}V	4.9	3.743 (5) m	1434	$2.8(2) \times 10^{-11}$
^{55}Mn (n,γ)^{56}Mn	13.3	2.579 (1) h	847	$5.0(3) \times 10^{-11}$
^{59}Co (n,γ)^{60}Co	16.5	1925.3 (1) d	1332	$1.6(6) \times 10^{-10}$
^{63}Cu (n,γ)^{64}Cu	4.5	12.701 (2) h	1346	$1.9(2) \times 10^{-11}$
^{107}Ag (n,γ)^{108}Ag	35	2.38 (1) m	633	$8.1(9) \times 10^{-10}$
^{108}Pd (n,γ)^{109}Pd	8.5	13.701 (2) h	311	$5.0(5) \times 10^{-11}$
^{113}In (n,γ)$^{114\,m}$In	8.1	49.51 (1) d	558	$5.0(3) \times 10^{-11}$
^{115}In (n,γ)^{116}In	73	54.3 (2) m	1294	$3.2(3) \times 10^{-9}$
^{115}In (n,n′)$^{115\,m}$In		4.468 (4) h	497	$9.8(9) \times 10^{-14}$
^{114}Cd (n,γ)^{115}Cd	0.29	53.46 (5) h	528	$1.2(1) \times 10^{-12}$
^{116}Cd (n,γ)^{117}Cd	0.052	2.49 (4) h	273	$3.0(1) \times 10^{-13}$

where $P(A_i^{\infty}|\phi_j)$ is the likelihood function representing the probability of obtaining A_i^{∞} due to ϕ_j. In this case the likelihood function is equal to the neutron cross section σ_{ij}. Hence, the obtained *a posteriori* probability can be fed back as an *a priori* information, resulting into an iterative method (Cvachovec and Cvachovec,) to unfold the neutron flux at bin j from the Eq. (1),

$$\phi_j^{(s+1)} = \frac{1}{\sum_{i=1}^{m}\sigma_{ij}} \sum_{i=1}^{m} \frac{\sigma_{ij}\phi_j^{(s)}A_i^{\infty}}{\sum_{k=1}^{n}\sigma_{ik}\phi_k^{(s)}}. \tag{5}$$

The advantage of using Bayes' unfolding method to solve the inverse problem in comparison to other methods used in Refs. Bitelli (2009); Iqbal (2009) lays in the possibility to start iterations with a uniform distribution for ϕ_j, or a reasonable guess as an *a priori* probability (D'Agostini, 1995).

4. Neutron reaction cross sections

Neutron reaction cross sections were obtained from the evaluated nuclear data bases ENDF/B.VII.1 (Chadwick, 2011), TENDL2014 (Koning, 2012) and JEFF-3.2 (The JEFF Team,). Using the software JANIS 4.0 provided by the Nuclear Energy Agency (NEA) it was possible to obtain each of the cross sections in Table 2, discretized in 10^4 isolethargic energy regions per decade. In the analysis we have succeeded in modifying the number of energy bin groups, adjusting them as needed. In Fig. 2 we present the cross section as function of the energy in the 10^4 isoletargic bins per decade (in red) and in 30 isoletargic energy bin groups (in blue).

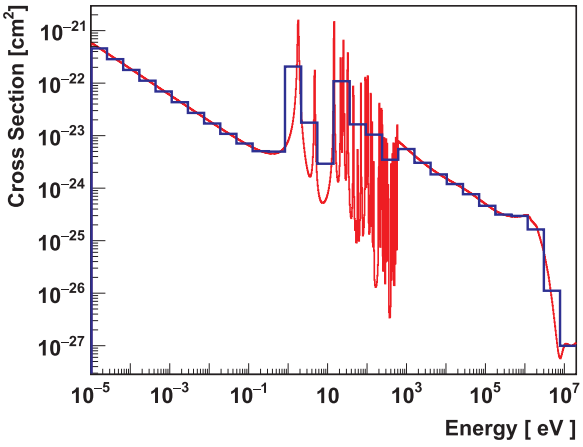

Fig. 2. ^{113}In(n,γ)^{114}In ENDF/B.VII.1 cross section. In red the cross section is shown the 10^4 isolethargic energy bin groups per decade. In blue is shown the cross section in 30 isolethargic energy groups. (For interpretation of the references to color in this figure legend, the reader is referred to the web version of this article).

5. Neutron self-shielding factor

When samples are immersed under a neutron flux, its interior gets exposed to a less neutron fluence rate than the exterior due to neutron absorption and scattering by the sample itself. This effect, known as neutron self-shielding, varies with the macroscopic scattering, absorption cross-sections, as well as size and shape of the sample (Greenberg, 2011). In neutron activation analysis, a self-shielding factor is applied as a correction to the saturation activity (Chilian, 2006), assuming that the neutron flux has mainly two components: thermal and epithermal. This is a strong assumption because it neglects the fast neutron contribution. In contrast, in the present work, we use the whole information available in the data bases. This is done in the following way a self-shielding factor is defined as the ratio between the neutron flux inside a sample $\psi(\mathbf{r}, \mathbf{\Omega}, E)$ with density ρ and volume V, and the neutron flux $\psi'(\mathbf{r}, \mathbf{\Omega}, E)$ inside a diluted sample with the same volume V and density $\rho_0 \sim 10^{-6}\rho$:

$$G = \frac{\int_E \int_{4\pi} \int_V \psi(\mathbf{r}, \mathbf{\Omega}, E)\, dVd\Omega dE}{\int_E \int_{4\pi} \int_V \psi'(\mathbf{r}, \mathbf{\Omega}, E)\, dVd\Omega dE}. \tag{6}$$

Now if a sample is immersed in a mono energetic neutron field with energy E_i, neutrons can experience an energy dispersion inside the sample due to several interactions of neutrons with the medium, namely $E_i \rightarrow E_j$. The neutron flux at energy E_j is now

$$\Psi_{i,j} \equiv \psi_i(E_j) = \int_{E_j} \int_{4\pi} \int_V \psi(\mathbf{r}, \mathbf{\Omega}, E)\, dVd\Omega dE. \tag{7}$$

Extending this idea to the n energy regions from the discretization of Eq. (1), the neutron flux inside the sample of volume V can be written in terms of its dispersion elements from Eq. (7). Therefore the flux inside the sample $\psi(\mathbf{r}, \mathbf{\Omega}, E)$, as well as the diluted sample $\psi'(\mathbf{r}, \mathbf{\Omega}, E)$, can be written as a matrix including the energy dispersion Φ and its matrix errors $\Delta\Phi$. The matrix elements ψ_{ij} and ψ'_{ij} can be obtained using Monte Carlo simulations.

The self-shielding and energy dispersion matrix elements $g_{i,j} = \frac{\psi_{i,j}}{\psi'_{i,j}}$ are calculated from the diluted flux $\psi'_{i,j}$ and non diluted flux $\psi_{i,j}$ matrix elements. To obtain each matrix element $g_{i,j}$ the Monte Carlo N-particle code MCNP6 was used. A mono-energetic 1 cm diameter spherical neutron source was simulated emitting neutrons isotropically inwards. The sample was located at the geometrical center of the sphere.

All the samples in Table 1 were simulated and the matrix elements of G were calculated. We have found that for all the simulated samples, the calculated non diagonal matrix elements of G were smaller by a factor 1000 relative to the diagonal elements. This means that geometry and thickness of the samples considered in this work the energy dispersion becomes negligible. Nonetheless self-shielding factors were obtained for all the j energy groups as illustrated in Fig. 3 where we can see the effect of resonances at epithermal neutron energies, which in the traditional way, i.e. taking the self-shielding factor an average over the complete energy space (Chilian, 2006), is not considered as a flux correction.

6. RECH-1 modeling and simulation

The RECH-1 research reactor is a pool-type reactor with a nominal thermal power of 5 MW. This reactor is operated by the Chilean Nuclear Energy Commission (a) at La Reina Nuclear Center. The RECH-1 is a light water-moderated, water-cooled and beryllium-reflected reactor and it employs a flat plate MTR-type fuel with low enriched uranium. Six blade-plates control absorbers pass through the core in three groups of two (Medel, 2003).

The neutron flux spectrum at the Vertical Dry Tube Irradiation

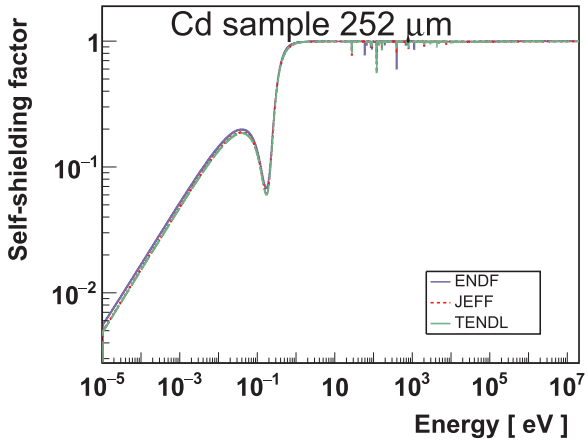

Fig. 3. Cadmium sample self-shielding factor curve for 1000 isolethargic energy groups, calculated using MCNP6 and three different neutron data bases.

Facility of the RECH-1 was calculated using MCNP6.1 (Goorley, 2012).

In order to perform the calculations for the RECH-1 applying the MCNP code, a methodology has been developed to be adapted to different situations and reactor states. The model includes irradiation devices and experimental sites, considering details that could affect the criticality calculations, neutron flux and power distributions. In Fig. 4 we illustrate the core components of RECH-1 and terminals of the pneumatic transport system (Rabbit Tubes), modeled in detail in three dimensions (Medel, 2003).

A *kcode* criticality source card was used to perform the criticality calculations. The number of *keff* cycles was 1000 with 10,000 neutrons per *keff* cycle. The neutron flux was calculated using *tally* F4, flux averaged over a cell. The cell was a sphere of radius 3 cm, whose center was located on the maximum of the axial neutron flux which is approximately 26.7 cm from the bottom of the active length of the fuel element, when the control plates of the reactor are 70% withdrawn. The resulting neutron flux spectrum is shown in Fig. 5.

7. Experimental results

The neutron flux in the Dry Tube irradiation position was obtained by: *a)* the atom-specific saturation activity shown in Table 2; *b)* Three different neutron data bases ENDF/B.VII.1 (Chadwick, 2011), TENDL2014 (Koning, 2012) and JEFF3.2 (The JEFF Team,) (see Sec. 4); and *c)* the EM method we have discussed above in Sec. 3, corrected by the neutron self-shielding factor. An important consideration is the state of knowledge of the reactor neutron flux at the Dry Tube irradiation position. This information was used to start the iterative process $\phi_j^{(s=0)}$ either with a uniform flux distribution (no knowledge), or with a

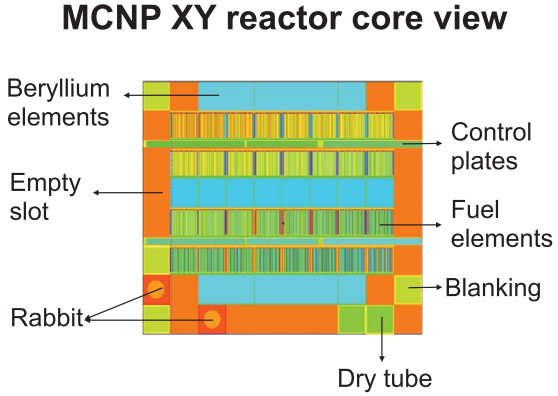

Fig. 4. RECH-1 MCNP simulation core scheme. Fuel elements, irradiation positions and other elements present at the reactor core are presented here.

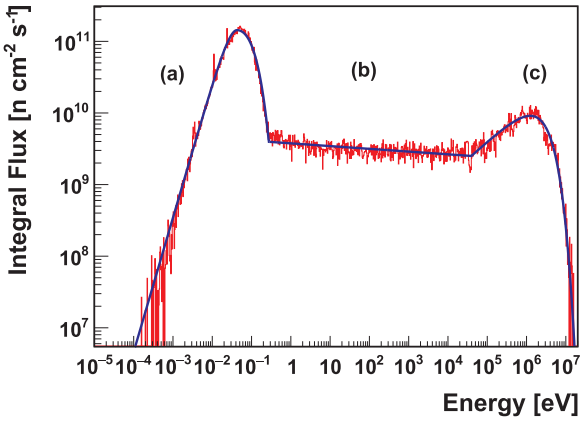

Fig. 5. RECH-1 MCNP simulated neutron flux distribution at Dry Tube position (in red), fitted with a parametrized three region neutron flux distribution: Thermal neutron distribution (Westcott, 1955) (a), epithermal neutron distribution (Westcott, 1955) (b), and Fast neutron distribution (Watt, 1952)(c). Fitting parameters of blue curves are shown in Table 3. (For interpretation of the references to color in this figure legend, the reader is referred to the web version of this article.)

parametrized neutron flux function following the usual three region neutron distribution. For the latter a Maxwell-Boltzmann (Westcott, 1955) distribution is used to describe the thermal region,

$$\Phi_{\text{th}}(E) = \text{A}\cdot\sqrt{\frac{1}{(k_B T)^3}}\cdot E\cdot\exp\left(-\frac{E}{k_B T}\right), \tag{8}$$

while the epithermic region is described by $\Phi_{\text{ep}}(E) = 1/E^{\alpha}$ distribution (Westcott, 1955). For the fast neutron region the flux is described by the Watt distribution (Watt, 1952),

$$\Phi_{\text{fs}}(E) = \text{B}\cdot\exp\left(-\frac{E}{a}\right)\cdot\sinh(\sqrt{bE}). \tag{9}$$

In Fig. 5 we show the MCNP simulated neutron integral flux distribution at Dry Tube irradiation position in red. The blue curve is the joint neutron distribution matching the three forms stated above, fitting the MCNP simulation data. In Table 3 we show the parameters for the different regions

The parameters were obtained from neutron flux distribution of the MCNP simulation of the RECH-1 reactor core at the dry tube irradiation position (see Fig. 5). The simulated MCNP neutron flux distribution is in Fig. 5 and the corresponding 3-region integral fluxes are $\phi_{\text{th}} = 9.8(2)\times10^{12}\ \text{cm}^{-2}\,\text{s}^{-1}$, $\phi_{\text{ep}} = 1.8(1)\times10^{12}\ \text{cm}^{-2}\,\text{s}^{-1}$ and $\phi_{\text{fs}} = 6.5(6)\times10^{11}\ \text{cm}^{-2}\,\text{s}^{-1}$. The total neutron flux is $\phi_{\text{tot}} = 1.22(3)\times10^{13}\ \text{cm}^{-2}\,\text{s}^{-1}$. This values, as well as the shape of the neutron distribution will help comparing with the EM method integral values.

The EM method is an iterative method. There are two numbers to be define beforehand: the number of discrete n energy groups, and the number of iterations s (see Eq. (5)). These parameters are modified, seeking an optimum n and s determined by the minimization of the statistical parameter ξ^2 defined as

Table 3
Fitted parameters from Fig. 5 according to Eq. (8) and Eq. (9). UpTh and UpEp are the low and high energy limits for the epithermal region.

Distribution	Fitted parameter	Value
$\Phi_{\text{th}}(E)$	A	$8.05(1)\times10^{10}\ \text{cm}^{-2}\,\text{s}^{-1}$
	T	221.78 (1) °C
$\Phi_{\text{ep}}(E)$	UpTh	0.28 (1) eV
	UpEp	$3.95(1)\times10^{4}$ eV
$\Phi_{\text{fs}}(E)$	B	$7.25(1)\times10^{9}\ \text{cm}^{-2}\,\text{s}^{-1}$
	a	$1.21(1)\times10^{6}$ eV
	b	$3.11(1)\times10^{-6}\ \text{eV}^{-1}$

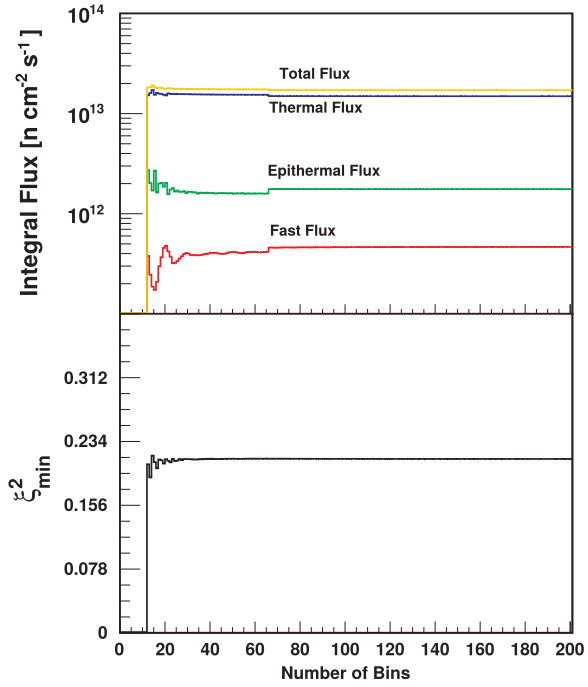

Fig. 6. Integral flux as a function of the number of bins when the number of iteration is set in order to minimize ξ^2. At the bottom is the value of ξ^2 as a function of the bin number.

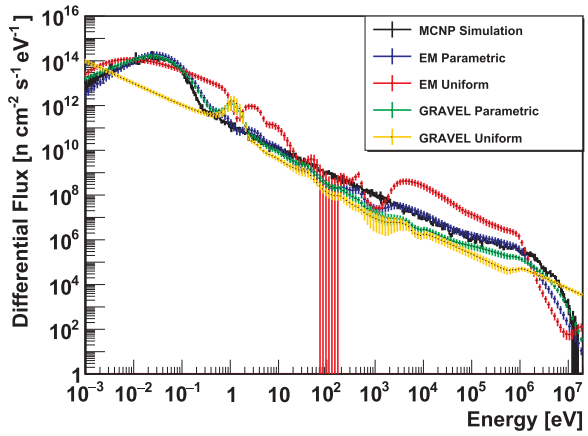

Fig. 7. Differential neutron flux as a function of the neutron energy, using the ENDF/B.VII.1 data base. Black curve is refer to MCNP simulation. Unfolding results (colored symbols) are not normalized. Uncertainty values were calculated for each energy bin group by Monte Carlo method (Cvachovec and Cvachovec,). (For interpretation of the references to color in this figure legend, the reader is referred to the web version of this article.)

$$\xi^2 = \frac{1}{m}\sum_{i=1}^{m}\left(\frac{A_i^{\infty} - A_i^{(s)\infty}}{A_i^{\infty}}\right)^2, \tag{10}$$

where A_i^{∞} is the measured saturation activity for reaction i; $A_i^{(s)\infty}$ is the calculated saturation activity for reaction i, using the EM calculated flux $\phi_j^{(s)}$ and the corresponding reaction cross section σ_{ij} ($A_i^{(s)\infty} = \sum_j \sigma_{ij}\phi_j^{(s)}$); and m is the total number of measured saturation activities considered.

The minimum ξ^2 was obtained seeking from $s = 0$, up to 100 iterations and $j = 15$, up to 200 isolethargic energy groups. As shown in Fig. 6 we notice that the value of ξ^2 exhibits a weak dependence on the number of energy regions n, when s minimizes ξ^2. The integral fluxes obtained using EM unfolding algorithm does not depend on n when is above sixty. Based on this results we have chosen to work with $n = 200$ hereafter.

In order to assess the unfolding flux results based on the EM algorithm, we have used the GRAVEL algorithm. This algorithm is an updated version of SAND-II, both are widely used to unfold neutron spectra from multi-foil neutron activation measurements. The GRAVEL algorithm was obtained from reference (Chen, 2014).

In Fig Fig 7 we present results for the differential neutron flux as a function of the energy. Uncertainty values were calculated by Monte Carlo method with random variations of the input data in the range of the uncertainties (Cvachovec and Cvachovec,) obtained for the atom-specific saturation activity, the self-shielding correction factor and the tabulated uncertainties of the reaction cross sections. For these results we have made use of three data bases and four unfolding algorithm. We observe a close agreement between the MCNP simulation and EM parametric at thermal and epithermal neutron energies (up to 1 MeV). Not surprisingly, the poorest agreement with MCNP simulation occurs with EM (red) and GRAVEL (yellow) unfolding algorithms using a uniform distribution as the starting profile. This is probably due to the fact that the starting condition is unrealistically far away from the real solution. MCNP simulation and GRAVEL parametric curves agree very well one with another at thermal neutron fluxes, although a clear disagreement is observed above 1 eV (epithermal and fast neutron fluxes). These findings point to the sensitivity of the unfolding results to the flux shape used in the first iteration of the algorithm.

In Table 4 we summarize integral neutron fluxes for the three energy regions considered: ϕ_{th}, ϕ_{ep} and ϕ_{fs}. We also show ξ^2_{min}, $\overline{\Delta}$ and σ_{STD}. Here ξ^2_{min} represents minimum statistical estimator value defined in Eq. (10). $\overline{\Delta}$ represents the average of the differences between the measured and the calculated saturation activities

$$\overline{\Delta} = \frac{1}{m}\sum_{i=1}^{m}(A_i^{\infty} - A_i^{(s)\infty}), \tag{11}$$

and σ_{STD} is the standard deviation for m measurements.

$$\sigma_{\text{STD}} = \sqrt{\frac{1}{m-1}\sum_{i=1}^{m}\left[\overline{\Delta} - (A_i^{\infty} - A_i^{(s)\infty})\right]^2}, \tag{12}$$

we observe that the EM Parametric procedure yields the highest maximum ξ^2_{min} and standard deviation, by a factor of 2 and 0.7 relative to GRAVEL Parametric. In addition, GRAVEL yields the lowest standard deviation ($\sigma_{\text{STD}} \approx 35$). This high value could be related to differences in the neutron fluxes during each measurement considering the long experimental campaign of eight months, where only one or two samples were able to be irradiated during the same week at 5 MW reactor operation power.

In Table 5 we present the weighed average for the neutron fluxes based on the three neutron data bases. We observe that at the thermal flux region GRAVEL and EM Parametric unfolding algorithms overestimate by 20–50% the flux relative to the MCNP simulation. At the epithermal region all Parametric unfolding procedures with MCNP results agree within their uncertainty values. In the fast flux region EM value is in closer agreement with the MCNP value, whereas GRAVEL underestimates the fast flux by nearly a factor of two.

From Table 5 it is possible to obtain the weighted average value of the integral fluxes in the thermal ($5 \times 10^{-5} - 0.5\,eV$), epithermal ($0.5 - 5 \times 10^5$ eV) and fast neutron ($5 \times 10^5 - 2 \times 10^7$ eV) energy regions for the three different databases.

8. Summary and conclusions

We have studied the neutron flux of an experimental nuclear reactor. In order to calculate the neutron flux at RECH-1 Dry Tube irradiaton position we have applied MCNP simulations and unfolding algorithms, together with experimental measurements. Special attention has been given to the self-shielding factor corrections. In addition we have modified the number of energy bins in the different regions of neutron cross sections, the self-shielding factor and neutron flux distribution in order to obtain the best fit of the data by the unfolding

Table 4
Summary of the integral neutron fluxes in three energy regions of interest using three data bases and four different unfolding algorithms: *I*) EM Uniform, *II*) EM Parametric, *III*) GRAVEL Uniform and *IV*) GRAVEL Parametric.

Data base	Algor.	bin	it	ϕ_{th} [$cm^{-2}s^{-1}$]	ϕ_{ep} [$cm^{-2}s^{-1}$]	ϕ_{fs} [$cm^{-2}s^{-1}$]	ξ^2_{min}	$\overline{\Delta}$	σ_{STD}
ENDF/B.VII.1	*I*	200	5	$1.3(4)\times10^{13}$	$1.6(6)\times10^{13}$	$1.4(5)\times10^{12}$	0.14	3.44	37.55
JEFF	*I*	200	4	$1.2(5)\times10^{13}$	$2.1(9)\times10^{13}$	$1.3(5)\times10^{12}$	0.20	− 3.70	44.04
TENDL	*I*	200	4	$1.2(4)\times10^{13}$	$1.8(6)\times10^{13}$	$1.0(3)\times10^{12}$	0.15	10.18	36.75
ENDF/B.VII.1	*II*	200	2	$1.5(6)\times10^{13}$	$1.8(7)\times10^{12}$	$4.7(19)\times10^{11}$	0.21	6.60	45.59
JEFF	*II*	200	2	$1.5(8)\times10^{13}$	$2.0(10)\times10^{12}$	$4.6(22)\times10^{11}$	0.30	0.01	54.33
TENDL	*II*	200	2	$1.5(7)\times10^{13}$	$1.9(8)\times10^{12}$	$4.0(16)\times10^{11}$	0.22	8.80	45.89
ENDF/B.VII.1	*III*	200	13	$1.1(3)\times10^{12}$	$1.7(10)\times10^{12}$	$2.2(7)\times10^{11}$	0.12	9.07	33.67
JEFF	*III*	200	18	$1.1(3)\times10^{12}$	$3.0(21)\times10^{12}$	$2.2(8)\times10^{11}$	0.15	4.03	38.29
TENDL	*III*	200	13	$1.1(3)\times10^{12}$	$1.7(11)\times10^{12}$	$2.1(7)\times10^{11}$	0.13	9.86	34.47
ENDF/B.VII.1	*IV*	200	10	$1.2(3)\times10^{13}$	$1.8(8)\times10^{12}$	$2.8(9)\times10^{11}$	0.12	9.27	33.71
JEFF	*IV*	200	2	$1.2(3)\times10^{13}$	$1.9(5)\times10^{12}$	$3.6(11)\times10^{11}$	0.15	5.30	38.07
TENDL	*IV*	200	9	$1.2(3)\times10^{13}$	$1.7(7)\times10^{12}$	$2.9(9)\times10^{11}$	0.13	10.13	34.47

Table 5
Weighted average of Thermal, Epithermal and Fast integral neutron fluxes for the three neutron databases.

Integral Flux	MCNP simulation	EM parametric	GRAVEL parametric	EM uniform	GRAVEL uniform
ϕ_{th} [$cm^{-2}s^{-1}$]	$9.8(2)\times10^{12}$	$1.5(4)\times10^{13}$	$1.2(2)\times10^{13}$	$1.3(2)\times10^{13}$	$1.1(2)\times10^{12}$
ϕ_{ep} [$cm^{-2}s^{-1}$]	$1.8(1)\times10^{12}$	$1.9(5)\times10^{12}$	$1.8(4)\times10^{12}$	$1.8(4)\times10^{13}$	$1.8(7)\times10^{12}$
ϕ_{fs} [$cm^{-2}s^{-1}$]	$6.5(6)\times10^{11}$	$4.3(11)\times10^{11}$	$3.0(6)\times10^{11}$	$1.2(2)\times10^{12}$	$2.1(4)\times10^{11}$

algorithms.

Using the EM parametric unfolding algorithm we obtained neutron fluxes at the Dry Tube of $1.5(4)\times10^{13}\ cm^{-2}\,s^{-1}$ for the thermal neutron energy region, $1.9(5)\times10^{12}\ cm^{-2}\,s^{-1}$ for the epithermal neutron energy region, and $4.3(11)\times10^{11}\ cm^{-2}\,s^{-1}$ for the fast neutron energy region. We have tested that the unfolding algorithms are sensitive to the information given in the first iteration, being the use of parametric three region neutron distribution the one which yields the most reliable integral flux results in comparison with MCNP simulations.

In this work we have been able to extend, for the first time, the use of the promising Expectation Maximization Bayes' algorithm to study reactor neutron flux distributions and it is presented as an alternative to well known unfolding methods such as GRAVEL, allowing to use the complete information available in nuclear data bases. Although the standard deviation of the calculated neutron flux distributions is relatively high when compared with the data, we would assume that this dispersion could be reduced if the neutron activation measurements were made in a shorter experimental campaign, perhaps one or two months; the energy distribution of neutron fluxes in a reactor depends on several factors that varies from one irradiation to another: freshness of the fuel, level of control rods, temperature of the pool water even if the core configuration remain the same during the whole experimental campaign.

Acknowledgments

The authors would like to thank the RECH-1 reactor crew including engineers, operators and technicians for their effort and valuable help during the experimental measurement campaign. We also thank to Prof. Dra. Berta Rubio for the enlightening discussions. FM acknowledges the support of CONICYT FONDECYT Iniciación 11130049. PA acknowledges to Beca CONICYT Doctorado D-21151450. JR-B acknowledges to Beca CONICYT Doctorado D-21151413. The authors would like to pay tribute to our colleague, teacher, advisor and friend Dr. José Roberto Morales Peña, who has recently passed away.

References

Bitelli, U., et al., 2009. Measurements of the neutron spectrum energy in the IPEN/MB-01 Reactor Core. Braz. J. Phys. 39 (1), 39–43. http://dx.doi.org/10.1590/S0103-97332009000100007.

Chadwick, M., et al., 2011. ENDF/B-VII.1: Nuclear data for science and technology: cross Sections, covariances, fission product yields and decay data. Nucl. Data Sheets 112, 2887.

Chen, Y., et al., 2014. Unfolding the fast neutron spectra of a BC501A liquid scintillation detector using GRAVEL method. Sci. China.: Phys. Mech. Astron. 57 (10), 1885–1890. http://dx.doi.org/10.1007/s11433-014-5553-7.

Chilian, C., et al., 2006. Dependence of thermal and epithermal neutron self-shielding on sample size and irradiation site. Nucl. Instrum. Methods Phys. Res. Sect. A: Accel. Spectrom. Detect. Assoc. Equip. 564 (2), 629–635. http://dx.doi.org/10.1016/j.nima.2006.04.026.(URL ⟨http://www.sciencedirect.com/science/article/pii/S0168900206006358⟩).

Cvachovec, J., Cvachovec, F. Maximum likelihood estimation of a neutron spectrum and associated uncertenties, Advances in Military Technology. 3 (2).

D'Agostini, G., 1995. A multidimensional unfolding method based on Bayes' theorem. Nucl. Instrum. Methods Phys. Res. A 362 (2–3), 487–498. http://dx.doi.org/10.1016/0168-9002(95)00274-X.

Goorley, T., et al., 2012. Initial MCNP6 release overview. Nucl. Technol. 180 (3), 298–315. http://dx.doi.org/10.13182/NT11-135.(URL ⟨http://www.ans.org/pubs/journals/nt/a_15346%5Cnpapers3://publication/doi/10.13182/NT11-135⟩).

Greenberg, R.R., et al., 2011. Neutron activation analysis: a primary method of measurement. Spectrochim. Acta Part B: At. Spectrosc. 66 (3–4), 193–241. http://dx.doi.org/10.1016/j.sab.2010.12.011.(URL ⟨http://dx.doi.org/10.1016/j.sab.2010.12.011⟩).

Hu, Z., et al., 1998. Energy and efficiency calibration of an array of six Euroball Cluster detectors used for beta-decay studies. Nucl. Instrum. Methods Phys. Res. Sect. A: Accel. Spectrom. Detect. Assoc. Equip. 419 (1), 121–131. http://dx.doi.org/10.1016/S0168-9002(98)01137-1.

Iqbal, M., et al., 2009. Development of computer software for Neutron energy spectrum adjustment in research reactors. Nucl. Technol. Radiat. Prot. 24 (1), 13–17. http://dx.doi.org/10.2298/NTRP09010131.

Jordan, D., et al., 2013. Measurement of the neutron background at the Canfranc Underground Laboratory LSC. Astropart. Phys. 42, 1–6. http://dx.doi.org/10.1016/j.astropartphys.2012.11.007.. URL ⟨http://dx.doi.org/10.1016/j.astropartphys.2012.11.007⟩.

Koning, A.D.R., 2012. Modern nuclear data evaluation with The TALYS code system. Nuclear Data Sheets 113, 2841.

Matzke, M. Unfolding of pulse high spectra. Technical Report PTB-N-24.

McElroy, W.N., et.al. Computer-automated iterative method for neutron flux spectra determination by foil activation, Vol. I: a study of the iterative method. Technical Report AFWL-TR-67-41.

Medel, J., et al., 2003. RECH-1 Reactor Conversion: a Core Characterization Formed by 32 Leu Fuel Element URL ⟨https://inis.iaea.org/search/search.aspx?Orig_q=RN:34083840⟩.

Roscoe, B.A., Furr, A.K., 1977. Time dependent deadtime and pile-up corrections for gamma ray spectroscopy. Nucl. Instrum. Methods 140 (2), 401–404. http://dx.doi.org/10.1016/0029-554X(77)90314-7.

Simonits, A., et al., 1975. Single-comparator methods in reactor neutron activation analysis. J. Radioanal. Chem. 24 (1), 31–46. http://dx.doi.org/10.1007/BF02514380.

Tain, J., Cano-Ott, D., 2007. Algorithms for the analysis of beta-decay total absorption spectra. Nucl. Instrum. Methods Phys. Res. Sect. A: Accel. Spectrom. Detect. Assoc. Equip. 571 (3), 728–738. http://dx.doi.org/10.1016/j.nima.2006.10.098.(URL ⟨http://linkinghub.elsevier.com/retrieve/pii/S0168900206018985⟩).

The JEFF Team, Jeff-3.2: Evaluated Nuclear Data Library.

Watt, B.E., 1952. Energy spectrum of neutrons from thermal fission of U235. Phys. Rev. 87 (6), 1037–1041. http://dx.doi.org/10.1103/PhysRev.87.1037.

Westcott, C., 1955. The specification of neutron flux and nuclear cross-sections in reactor calculations. J. Nucl. Energy 2, 59–76. http://dx.doi.org/10.1016/0891-3919(55)90017-6.

Zsolnay, E., Szondi, E. Experiences with the neutron spectrum unfolding code SANDBP. Report, BME-TR-RES-4/81. Nuclear Reactor of the Technical University of Budapest.